JACS
JOURNAL OF THE AMERICAN CHEMICAL SOCIETY
pubs.acs.org/JACS
Article

Enhanced Stabilization and Easy Phase Transfer of $CsPbBr_3$ Perovskite Quantum Dots Promoted by High-Affinity Polyzwitterionic Ligands

Sisi Wang, Liang Du, Zhicheng Jin, Yan Xin, and Hedi Mattoussi*

Cite This: J. Am. Chem. Soc. 2020, 142, 12669−12680
Read Online

ABSTRACT: The successful growth of colloidal lead halide perovskite quantum dots (PQDs) has generated tremendous interest in the community, due to the unique properties and the promise PQDs offer for use in applications involving light-emitting devices and solar cell technology. However, tangible progress in probing their fundamental properties and/or their integration into optoelectronic devices has been hampered by issues of colloidal and photophysical instability. Here, we introduce a promising surface coating strategy relying on a polyzwitterion polymer, where high-affinity binding onto the QDs is driven by multicoordinating electrostatic interactions with the ion-rich surfaces of $CsPbBr_3$ PQDs. The polymer ligands were synthesized by installing a stoichiometric mixture of amine-modified sulfobetaine anchors and solubilizing motifs on poly(isobutylene-*alt*-maleic anhydride), PIMA, via nucleophilic addition reaction. We find that this coating approach imparts enhanced colloidal and photophysical stability to the nanocrystals over a broad range of solvent conditions and in powder form. This approach also allows easy phase transfer of the PQDs from nonpolar media to an array of solutions with varying polarities and properties. Additionally, the stabilization strategy preserves the photophysical and structural characteristics of the nanocrystals over a period extending to 1.5 years under certain conditions.

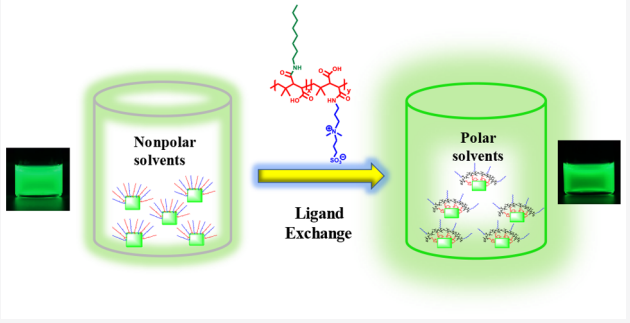

INTRODUCTION

Interest in metal halide perovskite materials has remarkably grown over the past few years.[1−5] Such interest has been motivated by the recent reported benefits of integrating these materials in applications that include solar cells and light-emitting devices.[1,6−10] The ability to prepare colloidal Cs-based perovskite nanocrystals (PQDs), using bottom up solution-phase growth routes, as first reported by Kovalenko and co-workers, has expanded that interest and generated much added activity.[11] The motivation to investigate and optimize the colloidal nanocrystal version of those materials is rooted in the great success made over the last three decades in developing "more conventional" colloidal quantum dots, such as core only and core−shell structures (e.g., CdSe, PbSe, CdSe-ZnS, and PbSe-ZnS).[12,13] Perovskite QDs exhibit a few unique and intriguing properties. Just like their oxide perovskite ancestors (e.g., $CaTiO_3$), PQDs are made of three-dimensional corner-sharing $[PbX_6]^{4-}$ octahedral structure.[5] In this structure, one or a mixture of large cations, namely, Cs^+, methylammonium ($CH_3NH_3^+$), or formamidinium ($CH(NH_2)_2^+$), occupy the large cavity between the octahedra (i.e., the A-site), which yields an overall composition of $APbX_3$. Only 3D polymorphs of the perovskite structure, either cubic or partially distorted variants, are semiconducting and offer the associated unique photophysical properties.[14] PQDs also exhibit narrow emission bands with broad color tunability, high charge-carrier mobility and long carrier lifetimes. The stoichiometry, size, and morphology of colloidal PQDs can be controlled by varying the type of precursor mix, ligand molecules, and the growth conditions used (e.g., temperature and solvent).[11,15] Additionally, $CsPbX_3$ nanocrystals exhibit high tolerance to structure defects, a very attractive property, as it endows these materials with high fluorescence properties without requiring electronic passivation of their surfaces.[3,16] Cumulatively, these properties have made $CsPbX_3$ PQDs very promising materials for use in optoelectronic devices, and for investigating photophysical processes involving energy and charge transfer interactions.[17−20]

However, a major hurdle that has inhibited in depth characterization of these materials and slowed potential technological developments has been attributed to their very

Received: April 4, 2020
Published: June 26, 2020

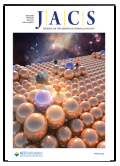

https://dx.doi.org/10.1021/jacs.0c03682
J. Am. Chem. Soc. 2020, 142, 12669−12680

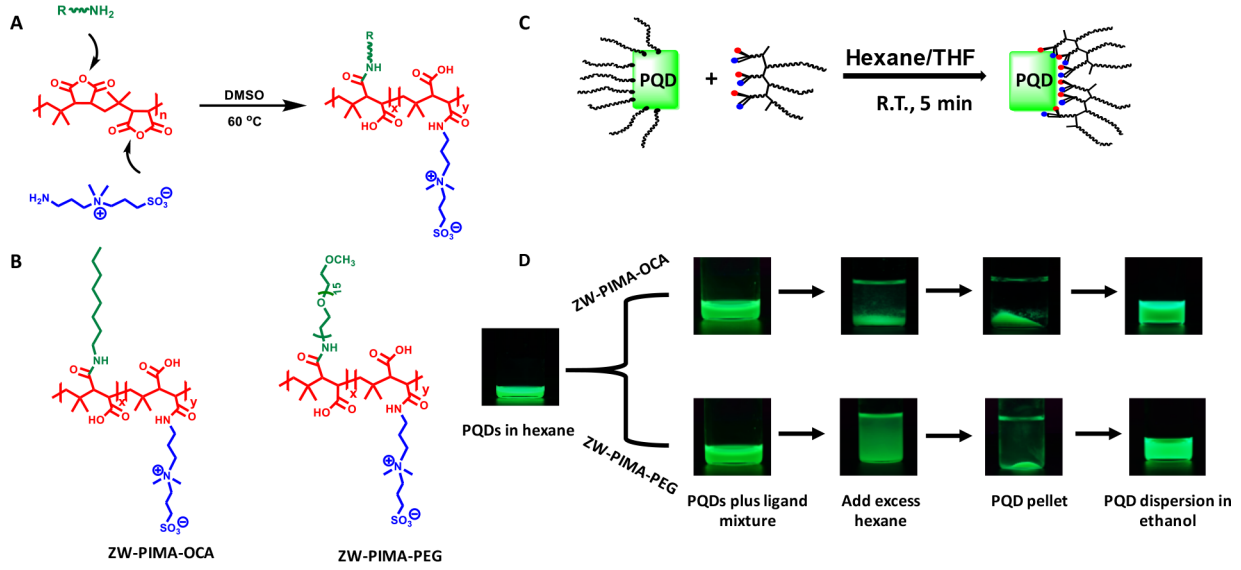

Figure 1. (A) Schematic representation of the one-step nucleophilic addition reaction used to prepare the multidentate zwitterion modified polymers starting with PIMA precursor. (B) Structures of two representative ligands are shown: ZW-PIMA-OCA and ZW-PIMA-PEG. (C) Schematic representation of the ligand exchange process. (D) Fluorescent images (collected using a hand-held UV lamp, with λ_{exc} = 365 nm) of PQDs during the ligand exchange steps with ZW-PIMA-OCA (top) or ZW-PIMA-PEG (bottom).

limited stability. Indeed, PQDs tend to degrade during storage, processing, or testing. They also lose their colloidal nature as well as absorption and emission features following exposure to polar media, such as alcohols and water.[14,21−23] It is believed that the ionic nature of the cores combined with a rather weak coordination of the native capping molecules (e.g., oleylamine (OLA) and oleic acid (OA), used during nanocrystal growth) and a high on/off rate of desorption contribute to their very limited stability.[24] This has led to much research in the field to develop alternative ligand chemistries that can enhance the colloidal stability of these materials. Ideas explored include the following: (1) introducing additional ligand species such as alkyl-zwitterion molecules or octylphosphonic acid during growth; (2) ligand exchange with small molecules such as didodecyl dimethylammonium bromide (DDAB) or with bidentate 2,2′-iminodibenzoic acid (IDA); and (3) embedding PQDs within a protective macroscale coating such as polystyrene matrix, or developing a protective polyhedral oligomeric silsesquioxane (POSS) cage around the QDs.[9,22,25−30]

Our group has recently developed a series of high-affinity metal-coordinating polymers as ligands to enhance the colloidal and photophysical stability of various inorganic nanocrystals.[31−36] Our design exploits the effectiveness of the nucleophilic addition reaction between poly(isobutylene-*alt*-maleic anhydride) (PIMA) copolymer and functional nucleophiles, to yield a series of multifunctional polymers that present several metal-coordinating groups (e.g., imidazole, thiol, or phosphonate), along with poly(ethylene glycol) (PEG) blocks or zwitterion motifs for promoting hydrophilicity of the polymer-coated nanomaterials. Using this design, a variety of colloidal QDs, plasmonic nanomaterials, and magnetic nanoparticles with excellent photophysical properties and remarkable stability have been prepared and tested.[31−36]

We thus reasoned that this route would allow the design of high-affinity ligands that are optimally adapted to provide much stability to the perovskite quantum dots. However, to be effective this chemical approach has to consider the salt nature of the perovskite cores, where strong coordination toward ion-rich surfaces is required. Additionally, we explored ligands that would potentially be useful for integrating the PQDs into electronic and light-emitting devices. Such ligands should present solubilizing motifs that can facilitate thin film processing and the transport of charge carriers.

In this report, we introduce a new set of coordinating polymer ligands that simultaneously present alkyl chains and zwitterion groups laterally arrayed along the backbone and use them as high-affinity coatings for the stabilization of $CsPbBr_3$ PQDs in a variety of polar solvents and for extended periods of time. The polymer synthesis relies on the highly effective nucleophilic addition reaction, to install several sulfobetaine zwitterion (SB-ZW) groups as anchors, along with multiple alkyl chains as solubilizing blocks. Since zwitterions combine Lewis acid and Lewis base moieties in their motifs, they can simultaneously interact with anions and cations on the PQDs. Furthermore, they can benefit from the chelating effects of having multiple SB groups per ligand, which achieves high-affinity coordination onto the PQDs.[27,28,37] A polymer presenting a mixture of SB-ZW and short PEG solubilizing blocks was also prepared and tested to provide a reference. Ligands with varying stoichiometry were prepared, wherein the fraction of zwitterion groups with respect to the alkyl chains per macromolecule could be varied. These ligands were tested for the stabilization of $CsPbBr_3$ PQDs grown using high temperature route. Our results have shown remarkable promise in promoting the colloidal stability of these materials under a wide range of conditions, allowing multiple washes and transfer between nonpolar and polar media. This could be achieved while preserving the nanocrystal integrity as well as the photophysical properties of these materials.

RESULTS AND DISCUSSION

Figure 1A,B schematically summarizes the ring-opening reaction and conditions used, along with the chemical structures of two sets of SB zwitterion-modified polymers:

https://dx.doi.org/10.1021/jacs.0c03682
J. Am. Chem. Soc. 2020, 142, 12669−12680

one presents lateral alky chains as solubilizing functions, while the other is made of PEG-ylated solubilizing moieties. Both sets of ligands are prepared by reacting the PIMA precursor with either a mixture of NH_2-ZW and octylamine (ZW-PIMA-OCA) or a mixture of NH_2-ZW and NH_2-PEG (ZW-PIMA-PEG) nucleophiles. The ring-opening reaction was carried out overnight under gentle heating conditions. With the precursor stoichiometry utilized, the two sets of polymers are expected to present ∼8 or 4 SB-ZW groups and ∼31 alky chains (for ZW-PIMA-OCA), and ∼8 SB-ZW and 31 PEG_{750} (for ZW-PIMA-PEG). Additionally, this reaction yields ∼40 carboxylic acid groups per chain.[32,35] The stoichiometry of both sets of ligands was quantified using solution-phase ^{1}H NMR spectroscopy (representative spectra are provided in the Figure S1). Excellent agreement between the nominal values and those extracted from NMR data is found (see Table 1). This

Table 1. List of Polymer Ligands Prepared and Tested for the Stabilization of $CsPbBr_3$ QDs[a]

ligand	molar fractions of SB versus solubilizing R groups used	number of SB and R groups per chain; nominal value[b]	number of SB and R groups per chain; measured value[c]
PIMA-OCA	0:80	SB-ZW = 0, OCA = 31	SB-ZW = 0, OCA ∼ 32
ZW-PIMA-OCA	10:80	SB-ZW = 4, OCA = 31	SB-ZW ∼ 4, OCA ∼ 31
ZW-PIMA-OCA	20:80	SB-ZW = 8, OCA = 31	SB-ZW ∼ 8, OCA ∼ 32
ZW-PIMA-PEG	20:80	SB-ZW = 8, PEG = 31	SB-ZW ∼ 7, PEG ∼ 32

[a]The relative molar fractions of the starting nucleophiles are shown with respect to the PIMA polymer, compared side-by-side with the measured values using NMR spectroscopy. [b]The reported values were obtained from the molar concentration of the amine-modified precursors, compared to that of the monomers in the PIMA. [c]The values were obtained by comparing the ^{1}H NMR peak integration of ZW (δ ∼2.0 ppm), OCA (δ ∼1.44 ppm) and PEG methoxy protons (δ ∼3.31 ppm) to the methyl groups in the polymer backbone (∼234 H, δ ∼0.97 ppm).

supports prior results from our group on other ligand systems and ultimately proves the efficiency of the nucleophilic addition reaction used.[32,35] Details about the synthesis, purification of the polymer compounds are provided in the Experimental Section.

The effectiveness of the polymer ligands was tested using a set of $CsPbBr_3$ PQDs grown following the reaction steps reported by Kovalenko's group, but with a few minor changes (see the Experimental Section).[11] The obtained nanocrystals, denoted as OA/OLA−PQDs, are stored as stock dispersions in hexane with concentration of ∼5 μM. The latter was calculated using a molar absorption coefficient, ε_{335}, of ∼0.042 d^3 μM^{-1} cm^{-1},[38] where d is the cube edge length (in nm) determined from high-angle-annular-dark-field scanning transmission electron microscopy (HAADF-STEM) data.

Ligand exchange with the polymers was carried out using one phase route and involved a few steps (as summarized in Figure 1C,D and Table 2). As a representative example, we describe ligand exchange with ZW-PIMA-OCA. First, PQDs dispersed in hexane and ZW-modified polymers dissolved in THF were mixed, yielding a clear solution, which was further stirred for ∼5 min. Excess hexane (∼2 mL) was then added, which turned the content turbid, indicating a loss of solubility

Table 2. Summary of the Minimum Amount of Ligands Required to Promote Ligand Exchange and Phase Transfer to Polar Media[a]

ligand	amounts of ligands required for phase transfer	phase transfer; stability
PIMA-OCA	∼25 mg	only partial phase transfer; no extended stability
ZW-PIMA-OCA (10%)	∼10 mg	full; stability ≥4 months
ZW-PIMA-OCA (20%)	∼5 mg	full; stability ≥8 months to 1.5 years
ZW-PIMA-PEG (20%)	∼15 mg	full; stability ∼2 months

[a]Also shown is the range of stability achieved for the resulting PQDs in polar solvents. An aliquot of the native PQD dispersion (200 μL, 5 μM) was used.

of the PQDs. Such a macroscopically visible change in the nanocrystal solubility provides the first proof of a successful competitive displacement of the native OA and OLA ligands and coordination of the ZW-containing polymers onto the PQDs. Following one round of centrifugation at 3500 rpm for 5 min, a fluorescent pellet was formed at the bottom of the vial, leaving a completely clear supernatant phase (see Figure 1D). The supernatant was discarded, and the PQD pellet was redispersed in THF and precipitated with excess hexane, followed by centrifugation. The procedure was repeated one or two more times as needed. The resulting fluorescent pellet was dried under vacuum, dispersed in the desired organic solvent, and used for further investigation. The above rounds of precipitation and centrifugation steps should guarantee a removal of the native OA and OLA capping species. Additional details on the ligand exchange are provided in the Experimental Section.

We would like to stress that excess free OA and OLA ligands were not removed from the PQD dispersion by washing with polar solvent and centrifugation prior to performing the ligand-exchange steps, as often done for conventional QDs and other colloids.[32,39,40] Including this step tends to negatively affect the integrity of the starting nanocrystals, making the ligand exchange with the new polymer less effective.

To be effective a ligand exchange with the new polymer requires a threshold ligand excess. For example, at least ∼1000× molar excess of ligand, with respect to nanocrystals, for a polymer presenting ∼4 SB-ZW group per chain; that amount can be reduced to ∼500× molar excess for a polymer presenting ∼8 SB-ZW groups per ligand (see Table 2). Additionally, ligand exchange with our polymer is rapid, requiring ∼5 min (or less) mixing, to provide polymer-stabilized PQDs; overall, we see no improvement in the final product when longer incubation time (up to 24 h while stirring) are used. This contrasts with the need for longer mixing time before sample processing for conventional nanocrystals (e.g., CdSe-ZnS QDs require a few hours using dihydrolipoic acid and ∼25−30 min using photoligation with lipoic acid ligands).[41,42] The relatively rapid ligand exchange process can be attributed to the rather labile binding of OLA and OA, compared to the higher affinity exhibited by the polyzwitterion ligands. We carried out a control experiment where ligand exchange was performed using PIMA-OCA (no SB, Table 2, row 1), in order to verify whether or not the carboxyl groups along the backbone can promote coordination onto, or encapsulation of the nanocrystals. We found that

https://dx.doi.org/10.1021/jacs.0c03682
J. Am. Chem. Soc. 2020, 142, 12669−12680

PIMA-OCA could not fully promote ligand exchange even when a larger molar excess was used (e.g., ∼5 times larger than ZW-PIMA-OCA). Furthermore, the resulting sample turned yellowish and progressively aggregated when dispersed in ethanol, along with a complete PL loss after 2−4 days.

Following these steps, the ZW-PIMA-OCA/PEG-capped PQDs were dispersed in several organic solvents including THF, chloroform, acetone, ethanol, 1-propanol, and 1-butanol and characterized using absorption and fluorescence spectroscopy, X-ray diffraction (XRD), and TEM. Characterization also probed the nature and structure of the coating using FT-IR and ^{1}H NMR measurements. Additionally, long-term colloidal stability tests spanning a period extending up to 1.5 years were carried out.

The photophysical properties of the polymer-coated PQDs were characterized and compared side-by-side to those collected from the starting OA/OLA-capped nanocrystals in hexane. Characterization centered on probing changes in the UV−vis absorption, as well as steady-state and time-resolved fluorescence spectra. Figure 2A shows the absorption profiles

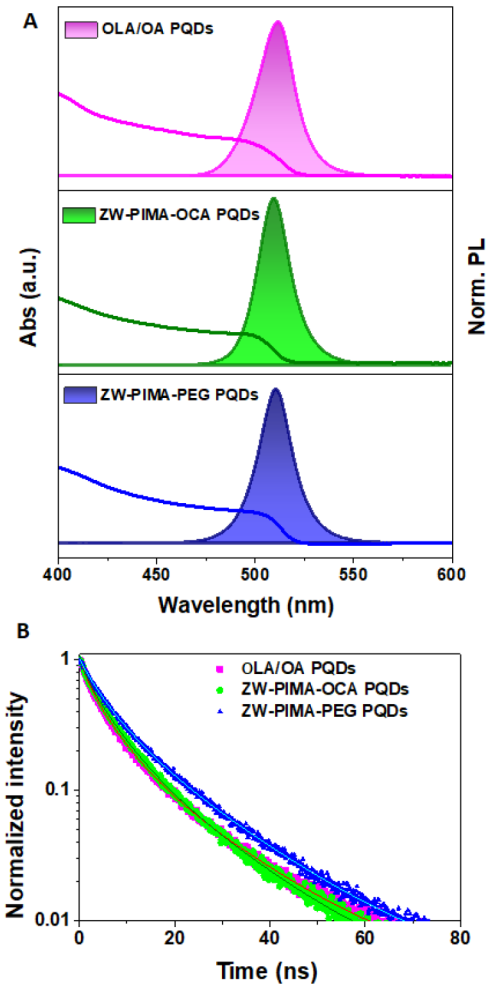

Figure 2. (A) Absorbance and photoluminescence spectra collected from dispersions of $CsPbBr_3$ QDs coated with the native ligands in hexane along with the nanocrystals coated with the two sets of ZW-PIMA-OCA and ZW-PIMA-PEG polymers in ethanol. The full width at half-maximum (fwhm) values are ∼25 nm (OLA/OA), ∼21 nm (ZW-PIMA-OCA), and ∼23 nm (ZW-PIMA-PEG). (B) PL lifetime decay profiles collected from dispersions of PQDs coated with OLA/OA, ZW-PIMA-OCA, and ZW-PIMA-PEG.

and photoluminescence spectra collected from three sets of $CsPbBr_3$ nanocrystals, namely, the native OA/OLA-capped PQDs in hexane as well as ZW-PIMA-OCA−PQDs and ZW-PIMA-PEG−PQDs in ethanol. Essentially identical spectra have been collected for the three samples, with clearly defined absorption edge at ∼500 nm and a narrow symmetric PL profile centered at ∼510 nm. Notably, there is a ∼1−2 nm shift in PL peak position after ligand exchange, a result similar to those reported in the literature when the native PQDs were exposed to thiocyanate salt or quaternary ammonium ligands.[43,44] Only a small change (∼2 ns) in the PL lifetime is measured for the ZW-PIMA-PEG−PQDs dispersed in ethanol (see Figure 2B and Table 3). Additional optical spectra

Table 3. Summary of the PL Lifetime and PL Quantum Yield Data[a]

ligand−PQDs	τ_{avg} (ns)	PL QY
OA/OLA−PQDs	7.0	0.55−0.60
ZW-PIMA-OCA−PQDs	7.6	0.65−0.75
ZW-PIMA-PEG−PQDs	9.2	0.70−0.80

[a]Data collected from OLA/OA−PQDs in hexane and ZW-PIMA-OCA/PEG coated PQDs in ethanol.

collected from dispersions in other polar solvents are provided in the Figure S2. The near-identical match between the absorption and emission spectra collected for the native nanocrystals and those ligated with the polymers implies that the electronic integrity of PQDs has been preserved after ligand exchange.

Next, we characterized the crystal structure and morphology of the PQDs before and after phase transfer. The powder XRD (PXRD) patterns collected from both as-prepared nanocrystals and after ligand exchange with the polymers are identical, proving that there are no signs of any phase transformation induced by the new ligand coating (see Figure 3A). These patterns correspond to a well-indexed standard cubic phase (Inorganic Crystal Structure Database (ICSD) card no. 29073).[11,45,46] Furthermore, our data show that no change in the diffraction pattern collected from the ZW-PIMA-OCA−PQD sample occurred during storage over the course of 1.5 years. This clearly confirms the high stability promoted by the polyzwitterion coating. We would like to stress that XRD patterns acquired from $CsPbBr_3$ nanocrystals have been fitted using cubic as well as orthorhombic crystal structures by different groups.[11,46−48] However, recent works by Brutchey and co-workers and Guagliardi and co-workers have suggested that data collected using synchrotron X-ray sources are better fitted using orthorhombic crystal structure.[49−51] In particular, they concluded that the ability to fit patterns measured by various groups using in-house (or benchtop) X-ray diffractometers, instead of synchrotron X-ray sources, can be attributed to size-broadening, a common property of colloidal nanocrystals, combined with modest signal-to-noise ratios for data acquired with in-lab experimental setups; these instruments tend to use much weaker X-ray beam sources. These factors have made data fitting to a simple cubic structure more suitable.

The XRD patterns collected from samples of ZW-PIMA-PEG-capped nanocrystals show a different progression with time (see Figure S3). Even though the pattern measured for the freshly prepared sample clearly exhibits characteristics of the cubic crystal phase, that pattern has changed with storage

https://dx.doi.org/10.1021/jacs.0c03682
J. Am. Chem. Soc. 2020, 142, 12669−12680

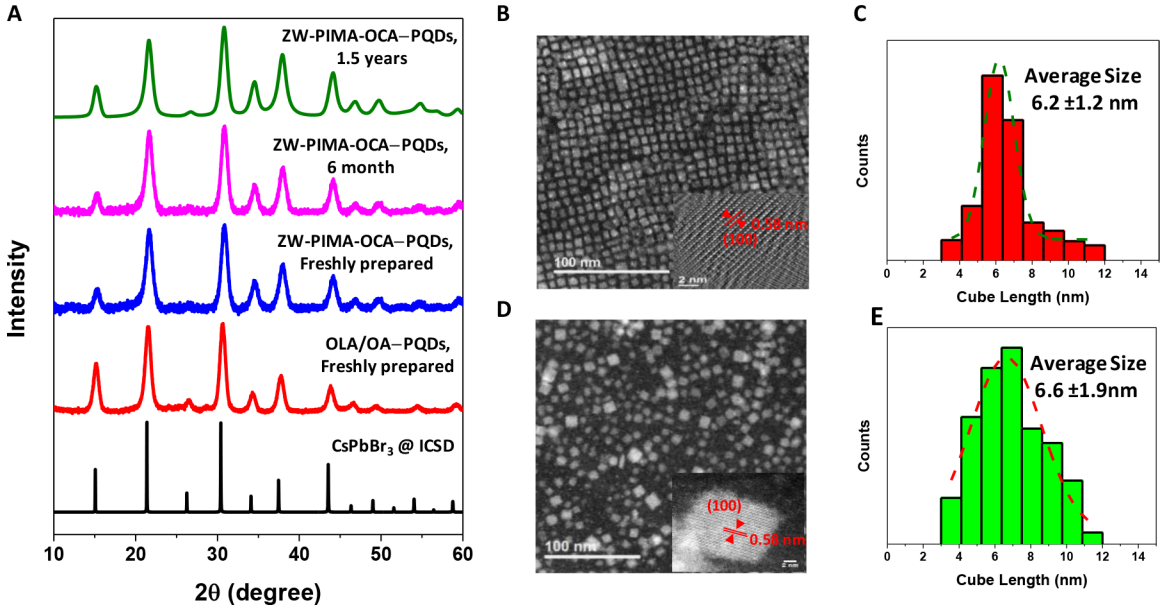

Figure 3. (A) Powder XRD patterns of OLA/OA–PQDs and ZW-PIMA-OCA–PQDs (freshly prepared or aged samples). The standard cubic phase is shown by ICSD card no. 29073. (B) STEM image and (C) size distribution histogram of OLA/OA–PQDs. (D) STEM image, and (E) size distribution histogram acquired from ZW-PIMA-OCA–PQDs. The insets in panels B and D show the HRSTEM image of PQDs with the spacing corresponding to the (100) crystal planes.

time. In particular, a new weak peak has emerged at $2\theta \sim 12°$, and the initial crystalline phase has essentially disappeared after 1 month, coupled with a complete loss of fluorescence. The ZW-PIMA-PEG–PQD dispersions in polar solvents also exhibit limited long-term stability compared to samples of ZW-PIMA-OCA–PQDs (see Figure S3). We attribute the inability of this polymer coating to impart long-term structural and photophysical stability onto PQDs to the nature of the PEG moieties. PEG blocks are polar in nature and can interact with the inorganic $CsPbBr_3$ cores, potentially affecting their integrity and photoemission properties.[52] To confirm this, we carried out a control experiment by mixing $CsPbBr_3$ NCs with a similar amount of PEG_{750}-OCH_3 blocks. A similar loss of structural order and fluorescence was measured within 1 month of storage (See Figure S4). This can be attributed to the fact that PEGylated polymers are hygroscopic and could absorb air moisture, resulting in progressive degradation of the perovskite nanostructures.[52,53] In contrast, ligands presenting alky chains are hydrophobic and thus provide better protection for the inorganic cores. Given this result, we limit the TEM characterization and stability experiments to ZW-PIMA-OCA–PQDs.

STEM data were used to probe the structural and morphological integrity of the PQDs after phase transfer. The TEM image in Figure 3B,C shows that the OLA/OA–PQDs have a cubic shape with an average edge length of ~6.2 ± 1.2 nm. Furthermore, the cubes tend to self-assemble during drying on a TEM grid. The STEM image acquired from the ZW-PIMA-OCA–PQDs also show cubic morphology, with an average edge size of ~6.6 ± 1.9 nm (Figure 3D,E). The high-resolution STEM (HRSTEM) images in the insets show resolved spacing between individual (100) crystal planes, with a lattice constant of 0.58 nm for both cases, which confirms that there is no loss in the core atom arrangements after ligand exchange, in agreement with the XRD data above and with literature results for OLA/OA–PQDs.[5,11] The slightly wider size distribution measured for the polymer-stabilized materials may be attributed to a mild rearrangement of the surface atoms induced by the drastic change in the nature, size, and affinity of the ligand during substitution. It is likely that a fraction of the surface atoms may have been briefly exposed (i.e., not passivated), which could induce small rearrangements of the outermost atomic layers, resulting in a broader size range for the polymer-coated materials. We also note that the image collected from the ZW-PIMA-OCA–PQDs shows no ordering (or self-assembly) of the NCs, in contrast to what was observed for the OLA/OA–PQD sample. This may also be attributed to the nature of the polymer coating, which is inherently polydisperse. It allows interpenetration between solubilizing moieties in adjacent QD coatings and eventually prevents self-assembly of the nanocrystals.

We now focus on the characterization of the coating molecules before and after ligand exchange and phase transfer (schematically represented in Figure 4A) and start with Fourier Transform infrared spectroscopy (FT-IR) measurements. The FT-IR spectra in Figure 4B show peaks centered at 2926, 2852, and 1465 cm^{-1} which are assigned to the C–H symmetric and asymmetric stretching and bending modes; these signatures are measured for both the native OLA/OA-coated and polyzwitterion-stabilized PQD samples.[54] Additionally, the peak around 1708 cm^{-1}, observed for both sets of samples, can be assigned to the carboxyl C=O stretching.[35,54] However, the broad bands centered at 3256 and 1567 cm^{-1}, respectively ascribed to the stretching and bending modes for O–H in the carboxyl group and N–H in the amide, are only present in the pure polymer and polymer-coated nanocrystals. Similarly, the strong peaks at 1171 and 1130 cm^{-1} assigned to S=O in the SB group are also only measured for the polymer-ligated sample.[55] Finally, the bands at 1642 and 991 cm^{-1}, which correspond to the C=C stretching and bending vibration modes, are absent from the polymer–PQD sample, indicating the successful substitution of the unsaturated alkene ligands with the new polymers.[56]

https://dx.doi.org/10.1021/jacs.0c03682
J. Am. Chem. Soc. 2020, 142, 12669–12680

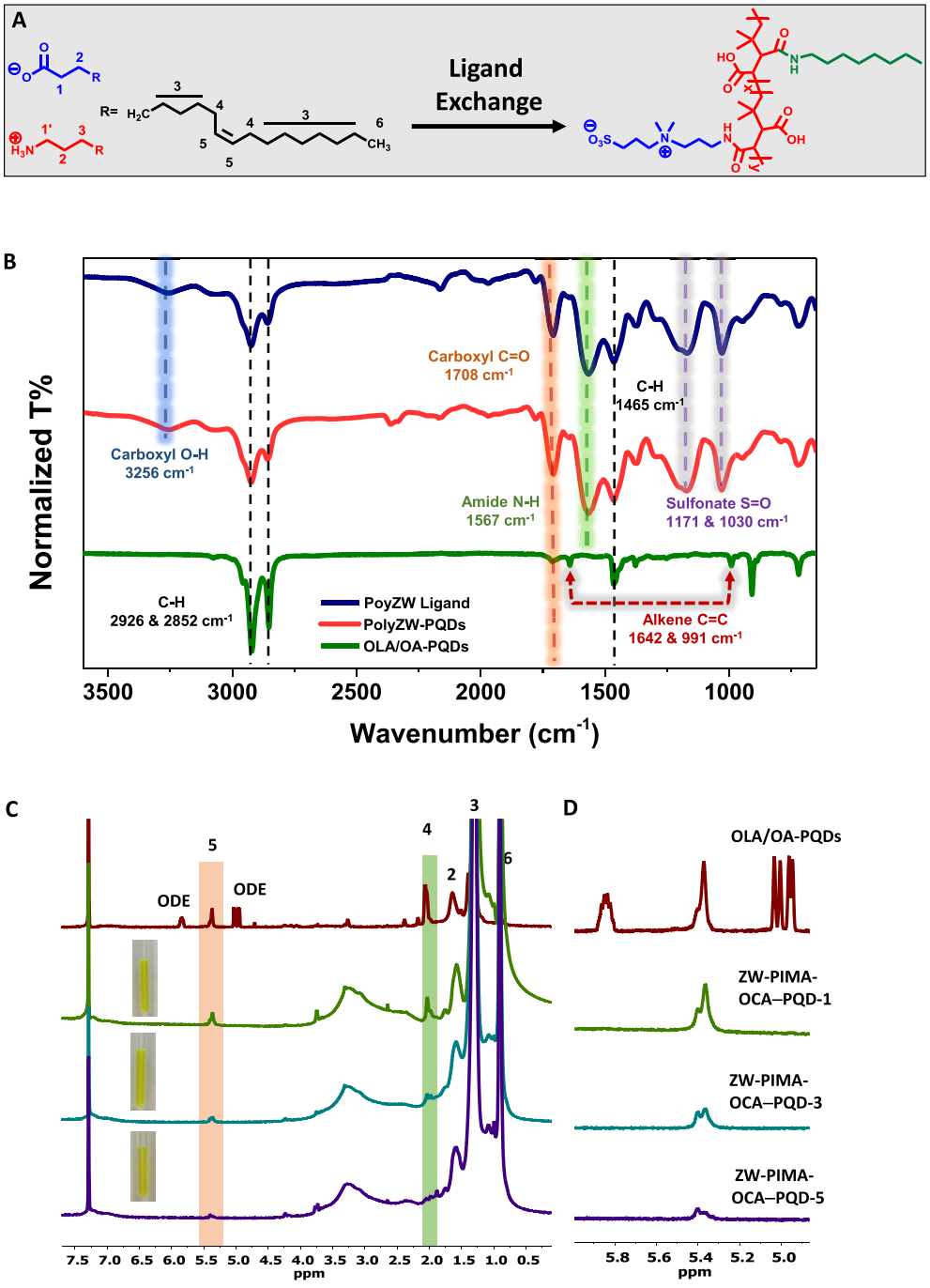

Figure 4. (A) Schematics representation of the capping molecules before and after ligand exchange. (B) FT-IR spectra collected from OLA/OA–PQDs and ZW-PIMA-OCA-coated PQDs and from the polymer ligand alone. (C) NMR spectra of PQDs before and after ligand exchange with ZW-PIMA-OCA subjected to different rounds of washing; insets show white-light images of the NMR tubes containing dispersions of ZW-PIMA-OCA–PQDs after each wash. (D) Expanded region of the NMR spectra focusing on the 5–6 ppm range is shown.

To further understand the progression of the ligand exchange, we utilized ^{1}H NMR spectroscopy to monitor changes in the composition of the coating shell, in a dispersion of polymer-coated PQDs in $CDCl_3$, through a few precipitation and redispersion cycles. The absence of any alkene resonances from the NMR spectrum of ZW-PIMA-OCA, allows us to exploit the 4–6 ppm region and track the removal of alkene-containing native cap during the ligand exchange and processing steps. Inspecting the spectra in Figure 4C,D allows us to identify the presence of both OLA/OA and ZW-PIMA-OCA ligands in the sample after ligand exchange and a few intermediate rounds of washing. Specifically, we assign the peaks at 5.37 ppm to the alkene resonance and the peak at 2 ppm to the CH_2 adjacent to the alkene double bond in OLA and OA, while the broad peak at 2.6–3.5 ppm emanates from the polymer ligand. We found that after three rounds of hexane washing, the remaining signatures in the ZW-PIMA-OCA–PQD NMR spectrum mainly emanate from the ligand, with essentially negligible signatures ascribed to the native molecules. After five washing cycles, the signal from the alkene resonance was reduced to below 3%, compared to that

https://dx.doi.org/10.1021/jacs.0c03682
J. Am. Chem. Soc. 2020, 142, 12669–12680

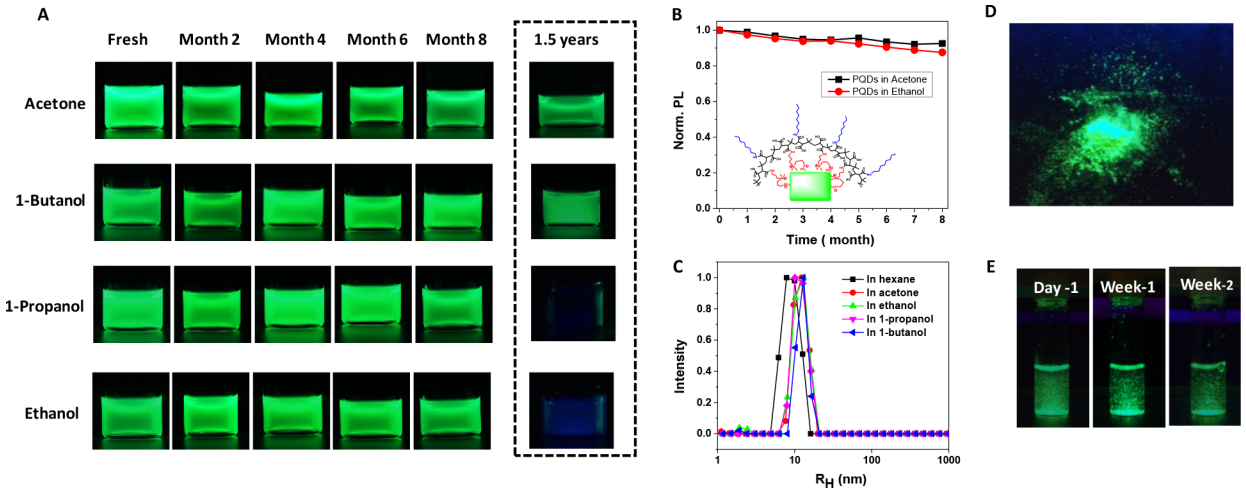

Figure 5. (A) Fluorescence images of ZW-PIMA-OCA−PQD dispersions in different polar solvents, UV illuminated using a hand-held UV lamp (excitation at 365 nm) and collected every month for a total period of 8 months; images from the same dispersions after 1.5 years of storage are also shown. (B) Plot of the PL intensity of ZW-PIMA-OCA−PQD dispersions in acetone and ethanol over the same 8 month period. (C) Histogram of the intensity vs hydrodynamic size distribution of OLA/OA−PQDs in hexane and ZW-PIMA-OCA−PQDs in acetone, ethanol, 1-propoanol, and 1-butanol. (D) Fluorescence image of a powder sample of ZW-PIMA-OCA−PQDs stored under atmospheric conditions for 12 months. (E) Fluorescence image of ZW-PIMA-OCA−PQD powder mixed with water (heterogeneous dispersion), freshly prepared and after 1 and 2 weeks. The fluorescence images shown in panels A, D, and E were collected using a Nikon D3300 camera, with the settings, an f/5.6 aperture and 1/20 s shutter speed.

of the starting sample, essentially confirming complete ligand exchange.

Having demonstrated that ligation of the polymer on the PQDs is rapid and promotes easy transfer to an array of polar solvents (or antisolvents), we now proceed to test the stability of ZW-PIMA-OCA−PQDs. Figure 5A shows a set of fluorescent images collected from dispersions of $CsPbBr_3$ nanocrystals (~1 μM) in acetone, ethanol, 1-propanol, and 1-butanol, either freshly prepared or during storage under ambient conditions, for a period of 8 months. The images show that the dispersions stay homogeneous and highly fluorescent throughout the test period. We stress that the dispersions in acetone and 1-butanol exhibit longer stability, as images collected after 1.5 years show bright and homogeneous samples. Emission is nonetheless essentially lost after 1.5 years from the two dispersions in ethanol and 1-propanol. Figure 5B shows a plot of the normalized PL intensity collected from dispersions in acetone and in ethanol over the 8 month period; less than 15% drop in the PL was measured. We should contrast this with the fact that dispersions of OLA/OA−PQDs in nonpolar solvents such as toluene or hexane progressively aggregate and lose most of their emission after ~1 month of storage. Dynamic light scattering (DLS) measurements have also been used to gain additional information on the hydrodynamic size of the coated PQDs, and to assess whether microscopic aggregation at any level has taken place during the ligand exchange steps. DLS measurements were applied to both OLA/OA− and ZW-PIMA-OCA−PQD dispersions. Figure 5C shows representative profiles of the intensity distribution of hydrodynamic size (R_H), extracted from the Laplace Transform of the autocorrelation function, $g^{(1)}$. Plots of $g^{(1)}$ versus log(τ), collected from dispersions of OLA/OA−PQDs in hexane and ZW-PIMA-OCA−PQDs in various polar solvents are provided in the Figure S5. Data show that the dispersions are indeed homogeneous, made of a single narrow population of nanocrystals with an average R_H of ~8.6 nm for OLA/OA−PQDs in hexane and ~11.9 nm for ZW-PIMA-OCA−PQDs in ethanol (see Table S1). The small increase in the measured R_H after ligand exchange (~3.3 nm) is attributed to the polymeric nature of the coating compared to molecular scale OLA/OA; they yield different hydrodynamic contributions to the Brownian diffusion of the materials.[57] The ZW-PIMA-OCA-stabilized nanocrystals can be dried and processed into a fine dry powder, where they maintain strong fluorescence after 1 year of storage under atmospheric conditions (see Figure 5D). We also tested the resistance of a powder sample of the polymer-coated PQDs exposed to a solution of DI water (see Figure 5E). The sample forms a heterogeneous suspension (as expected given the hydrophobicity of the polymer), which emits strong green fluorescence after 2 weeks of storage. Comparable results can be achieved only when embedding OA/OLA−PQDs within a protective polymer matrix.[22,30] Cumulatively, the high stability of the ZW-PIMA-OCA−PQDs under various conditions, both dispersed in polar media or in powder form, along with the resistance to water are attributed to the high affinity of the ligands to the PQD surfaces as well as the effective steric repulsions afforded by the polymer coating.

We now would like to discuss our findings and provide some perspective in comparison to prior works aimed at the stabilization of colloidal PQDs through ligand engineering. However preliminary these results may be, our coordinating polymer based on the SB-ZW anchoring motif provides remarkable improvements in the colloidal properties of $CsPbBr_3$ QDs in a wide range of solution conditions, while preserving or even enhancing their photophysical properties (see Figure 2 and Table 3). This result can be attributed to the better passivation afforded by the use of anchors simultaneously presenting Lewis acid (quaternary ammonium) and Lewis base (sulfonate), combined with higher ligand-to-nanocrystal affinity and reduced rate of desorption. The steric hindrance imparted by the alkyl-rich polymer coating can better protect the NCs and reduce the surface trap density. Additionally, because the sulfonate anion ($-SO_3^-$) is a soft

https://dx.doi.org/10.1021/jacs.0c03682
J. Am. Chem. Soc. 2020, 142, 12669−12680

Lewis base compared to the carboxylate (in OA^-), its coordination provides more effective passivation of the surface Pb^{2+} (soft Lewis acid) on the PQDs.[58]

Our coating strategy shares some aspects discussed in recent publications by Kovalenko's group who used molecular zwitterion, namely sulfobetaine and phosphocholine containing ligands.[27,28] They showed that introducing those compounds during the growth reaction yields improvement in the colloidal stability against washing with antisolvents and under high dilution, for example. A coordinating polymer based on SB and phosphocholine zwitterions, prepared via RAFT polymerization was recently used to impart stability of $CsPbBr_3$ NCs in nanocomposite films by Emrick and co-workers, with additional good resistance to water.[59] Earlier work by Kanaras and co-workers tested the effectiveness of incorporating poly(maleic anhydride alt-1-octadecene) (PMAO) during growth of OLA/OA−PQDs, to improve their stability, via entanglement with the OLA/OA molecules and reduction of the binding dynamics on the PQDs surface.[60] In a recent work, Manna and co-workers mixed PMAO with Cs_4PbBr_6 nanocrystals and allowed the ring-opening reaction between the succinic anhydride rings in the polymer chain and oleylamine species in the nanocrystal native coating. This reaction produces polysuccinamic acid coating, which triggers the conversion of those starting nanocrystals to polymer-protected $CsPbBr_3$ QDs and yields better colloidal stability.[61] These results indicate that the carboxyl groups, or derivatives of those, can interact with the $CsPbBr_3$ NCs. This finding is in good overall agreement with our present results, where we found that coordination of PIMA-OCA ligands onto the nanocrystals occurs. Nonetheless, binding is rather weak and cannot impart onto the NCs colloidal stability under polar conditions.

Finally, we would like to note that the present polymer design cannot allow the installation of larger fractions of SB groups than 8−10 groups per polymer ligand, due to the stringent solubility requirements imposed by these groups. Application of this ligand design to the red-emitting, iodide-based PQDs is less effective. We are exploring the use of polysalt structures, with control over the nature of the Lewis acid and Lewis base groups. We hope to elaborate on those results in future reports.

CONCLUSION

In summary, we have designed a set of polymers modified with several sulfobetaine groups and used them as high-affinity ligands that can competitively displace the native capping on $CsPbBr_3$ QD surfaces. The successful ligand exchange with these compounds ensures the rapid phase transfer of PQDs to several organic solvents, including those with high polarity, while preserving the structural, morphological, and photophysical integrity of the NCs. Furthermore, the polymer-stabilized PQDs exhibit great colloidal stability over a period extending to 1 year. Evidence for a strong interactions and binding of the polyzwitterion ligands onto the nanocrystals was confirmed using surface characterization measurements relying on FT-IR and NMR spectroscopy, which showed that a near-total removal of the native ligands was achieved. We attribute these highly promising findings to the architecture of the polymer platform, which presents multiple zwitterion groups. These guarantee the simultaneous presence of permanent cations and anions in a single polymer chain and promote electrostatic binding with both anions and cations on the PQD surfaces via Lewis acid−base type interactions. More precisely, $CsPbBr_3$ PQD surfaces are terminated with an outer shell of AX (with A being Cs^+ or OLA^+ and X being Br^- or OA^-) and an inner shell of $PbBr_2$ (made of Pb^{2+} and Br^- ions). We surmise that the quaternary ammonium and sulfonate groups along the polymer ligand can strongly coordinate onto the surface ions, displacing OLA^+ and OA^- and imparting enhanced stability to the PQDs.[58,62,63] Our results shed light on the subtle nature of the interactions of stabilizing ligands with the ion-rich surfaces of colloidal perovskite nanocrystals and bode well for potentially expanding the application of this design to PQDs with other core compositions. Our data can also facilitate the integration of these materials in practical applications involving, for example, display and energy conversion devices.

EXPERIMENTAL SECTION

Growth and Purification of $CsPbBr_3$ PQDs. *Growth of $CsPbBr_3$ PQDs.* Growth of the PQDs was carried out in our laboratory following literature protocols,[11] with minor adjustments. In a typical preparation, Cs-oleate precursor was first prepared by mixing Cs_2CO_3 (0.163 g, 0.5 mmol), 1.2 mL of oleic acid (OA), and 15 mL of octadecene (ODE) in a 50 mL three-necked round-bottomed flask. After degassing the mixture under vacuum at 120 °C for 1 h, the solution was heated to 150 °C under nitrogen atmosphere, yielding a clear solution of Cs-oleate, which can be stored under nitrogen atmosphere until further use. Separately, 0.138 g (0.376 mmol) of $PbBr_2$, 10 mL of ODE, 2 mL of OA, and 2 mL of OLA were loaded into a 50 mL three-necked round-bottomed flask, and the mixture was degassed at 120 °C for 1 h. Once dissolution of the $PbBr_2$ was complete (usually manifesting in the solution becoming clear), the mixture was switched to nitrogen atmosphere and further heated to 170 °C. Then, 0.6 mL of the above Cs-oleate stock solution preheated to ∼100 °C was rapidly injected via a syringe into the solution to initiate the growth of $CsPbBr_3$ QDs. After letting the mixture react for ∼5 s, the flask was immersed into an ice bath to quench the growth. During quenching, the solution color turned from light yellow to light green. We should note that maintaining the Cs-oleate precursor solution in ODE at ∼100 °C before injection is necessary, in order to avoid precipitation of Cs-oleate which occurs under room temperature conditions.

Purification of $CsPbBr_3$ PQDs. The crude solution of $CsPbBr_3$ PQDs was first centrifuged at 3600 rpm for 5 min. The precipitate was then dispersed in 2 mL of hexane under sonication and subjected to another round of centrifugation at 3600 rpm for 5 min. The clear supernatant was collected and diluted with the appropriate volume of hexane to yield a stock dispersion with concentration ∼5 μM. Those nanoparticles denoted as OLA/OA−PQDs were then used to carry out further characterization and studies.

Ligand Synthesis. The amine-modified nucleophile precursors required for the synthesis of the polymer were prepared in our laboratory following protocols described in previous reports. Synthesis of the amine-modified sulfobetaine zwitterion (NH_2-ZW) was carried out following reported literature protocols with minor modifications.[33,64] First, the primary amine group of the *N*,*N*-dimethylamino propylamine was protected by using di*tert*-butyl decarbonate (Boc), then the tertiary amine at the other end of the intermediate was coupled to 1,3-propane sultone. Last, the protecting Boc group was removed by acid (HCl) treatment to free the primary amine. We should note that an excess of HCl was added in the de-Boc process, which can protonate the resulting amine group. This could further reduce the effectiveness of the polymer addition reaction and introduce a minimum amount of Cl^- to the synthesized polyzwitterion ligand. The presence of Cl^- anions in the polymer ligand can cause a blueshift in the $CsPbBr_3$ PQD emission by promoting anion exchange with the nanocrystals during the ligand exchange process. To address this problem, we used triethylamine to remove the HCl from the NH_2-ZW. The formed triethylamine·HCl

https://dx.doi.org/10.1021/jacs.0c03682
J. Am. Chem. Soc. 2020, 142, 12669−12680

salt byproduct was discarded along with the supernatant during purification by using chloroform (as antisolvent) to wash the NH_2-ZW product. The amine-terminated poly(ethylene glycol) methyl ether (NH_2-PEG_{750}-OCH_3) was synthesized through azide modification of PEG methyl ether followed by amine transformation, as described in refs 42 and 65−67. The hydrophobic octylamine nucleophile was used as purchased. These nucleophiles were used in the synthesis of the polymer ligands via the nucleophilic addition reaction, as described below.

Synthesis of ZW-PIMA-OCA (20, 10, and 0%). The percentage refers to the fraction of monomers modified with sulfobetaine (SB) zwitterion groups along the PIMA backbone. We describe the preparation of the ligand presenting 20% SB-ZW moieties. In a 50 mL round-bottomed flask equipped with a magnetic stir bar, 0.5 g of PIMA (3.33 mmol of monomer units) was dissolved in 5 mL of DMSO and heated to 60 °C. A solution of NH_2-ZW (0.15 g, 0.67 mmol) in 2 mL of DMSO was added slowly to the PIMA. After stirring for 20 min, 2 mL of DMSO solution containing octylamine (0.44 mL, 2.66 mmol) was added, and the reaction mixture was left to stir at 60 °C overnight. The solvent was evaporated under vacuum, and the residual compound (as a white crystal) was dissolved in chloroform (4 mL). This concentrated ligand solution was then added dropwise to a flask containing 100 mL of hexane (a large excess) under vigorous stirring. This induced precipitation of the ligand as a white sticky solid. The supernatant was decanted, and the obtained white solid (product) was subjected to another round of dissolution in chloroform and precipitation using excess hexane. The final product was dried under vacuum at 40 °C (using a vacuum oven) for 5 h, yielding a white powder with reaction yield of ∼75%. Synthesis of ZW-PIMA-OCA (10%) or PIMA-OCA was carried out following the above protocol; only the amount of added NH_2-ZW was reduced from 0.67 to 0.34 mmol for ZW-PIMA-OCA (10% SB) or 0 mmol for PIMA-OCA. We should note that applying 2−3 rounds of dissolution of the ZW-PIMA-OCA polymer in acetone then precipitation with water would help removing traces of Cl^- ions from the compound, which eliminates potential complications caused by interaction of these ions with the PQDs during ligand substitution.

Synthesis of ZW-PIMA-PEG (20%). PIMA (0.5 g, 3.33 mmol of monomers) was dissolved in 5 mL of DMSO using a 50 mL round-bottomed flask equipped with a magnetic stir bar. To the stirring solution, 2 mL of DMSO containing NH_2-ZW (0.15 g, 0.67 mmol) was added dropwise. After 20 min of additional stirring, a solution of NH_2-PEG (1.98 g, ∼2.66 mmol) in 4 mL of DMSO was added, and the reaction mixture was left stirring at 60 °C overnight. The solvent was removed under vacuum, and chloroform (2 mL) was added to dissolve the crude product. The solution was then loaded onto a silica column, and the compound was purified with a mixture of chloroform/MeOH (9:1) as the eluent. The eluted aliquots were combined and dried under vacuum, yielding the final product (as a transparent gel); the overall yield was ∼80%.

Ligand Exchange and Phase Transfer. A stock dispersion of PQDs in hexane (200 μL, ∼5 μM) was loaded onto a 10 mL scintillation vial. Separately, 5 mg of ZW-PIMA-OCA (20%) or 15 mg of ZW-PIMA-PEG (20%) were dissolved in 200 or 400 μL of THF, respectively. The ligand solution was added to the vial containing the PQD dispersion, and the mixture was left stirring at room temperature for 5 min. The PQDs were then precipitated by the addition of 2 mL of hexane (an excess). Following sonication for ∼1 min, the solution was centrifuged at 3700 rpm for ∼5 min, yielding a green pellet. The clear supernatant was discarded, and the pellet was redispersed in 200 μL of THF, followed by another round of precipitation using excess hexane. The final precipitate was dried under vacuum for ∼10 min to yield either a green-yellowish powder (for PQDs ligated with ZW-PIMA-OCA) or a gel-like pellet (for PQDs ligated with ZW-PIMA-PEG). The isolated materials were then dispersed in 200 μL of different organic solvents including acetone, ethanol, 1-propanol, and 1-butanol for further use and characterization. We note that the ligand exchange procedure can be scaled up 10-fold without affecting the quality of the final materials.

Colloidal Stability Tests. The samples used for stability tests were prepared as follows. First, 100 μL aliquots of the polymer-modified PQD colloids were retrieved from the stock dispersions (in different polar solvents) and loaded onto 2 mL glass vials. Then, 400 μL of the corresponding solvent was added to adjust the nanocrystal concentration to ∼1 μM. All the samples were sealed and stored under room temperature conditions. Fluorescence images of the vials under UV illumination (using a hand-held UV lamp, excitation at 365 nm) were regularly taken. Similarly, to collect the absorption and photoluminescence spectra of the PQD dispersions in acetone and ethanol, a small volume of the stock dispersion was diluted in a Spectrocell with a 5 mm optical path to yield an optical density (OD) of ∼0.1 at 400 nm for all samples (i.e., the same PQD concentration). The ZW-PIMA-OCA−PQD powder sample was prepared using the same protocol described above, but the pellet was dried and "crushed" into a fine powder. For the water-resistance experiments, 5 mg of ZW-PIMA-OCA−PQD powder was added to 3 mL of DI water to form a heterogeneous suspension and fluorescence images were acquired over a 2-week period.

NMR Sample Preparation. Briefly, for the native nanocrystals, a 500 μL aliquot of OLA/OA−PQDs were retrieved from the stock dispersion and precipitated using ethyl acetate one time, then dried under vacuum. The sample was dispersed in 500 μL of $CDCl_3$, loaded onto an NMR tube, and the spectra were collected. For the ZW-PIMA-OCA−PQDs, an aliquot of OLA/OA−PQDs stock solution (500 μL) was ligand-exchanged with the ZW-PIMA-OCA polymer following the protocol described above. The dried PQDs pellet was dispersed in 500 μL of $CDCl_3$ after one round of precipitation using excess hexane, yielding sample ZW-PQD-1. The NMR samples ZW-PQD-3 and ZW-PQD-5 designate dispersions that have been subjected to three and five rounds of purification, using the steps described above, before redispersion in $CDCl_3$. These dispersions were used to collect the spectra shown in Figure 5C. All the ZW-PQD-*n* samples have similar concentrations. ^1H NMR spectra were collected using an average over 128 scans.

■ ASSOCIATED CONTENT

Supporting Information

The Supporting Information is available free of charge at https://pubs.acs.org/doi/10.1021/jacs.0c03682.

Additional information, Materials, Instrumentation, NMR spectra of sulfobetaine-modified polymer ligands, polymer-coated nanocrystals, powder XRD patterns, and colloidal stability tests (PDF)

■ AUTHOR INFORMATION

Corresponding Author

Hedi Mattoussi − *Florida State University, Department of Chemistry and Biochemistry, Tallahassee, Florida 32306, United States;* orcid.org/0000-0002-6511-9323; Email: mattoussi@chem.fsu.edu

Authors

Sisi Wang − *Florida State University, Department of Chemistry and Biochemistry, Tallahassee, Florida 32306, United States*

Liang Du − *Florida State University, Department of Chemistry and Biochemistry, Tallahassee, Florida 32306, United States*

Zhicheng Jin − *Florida State University, Department of Chemistry and Biochemistry, Tallahassee, Florida 32306, United States*

Yan Xin − *Florida State University, National High Magnetic Field Laboratory, Tallahassee, Florida 32310, United States*

Complete contact information is available at: https://pubs.acs.org/10.1021/jacs.0c03682

Notes

The authors declare no competing financial interest.

■ ACKNOWLEDGMENTS

The authors thank FSU and the National Science Foundation (NSF-CHE #1508501), AFOSR (Grant No. FA9550-18-1-0144), and Kasei-Asahi for financial support. TEM experiments were performed at the National High Magnetic Field Laboratory, which is supported by the National Science Foundation Cooperative Agreement No. DMR-1644779 and the State of Florida.

■ REFERENCES

(1) Tsai, H.; Nie, W.; Blancon, J.-C.; Stoumpos, C. C.; Asadpour, R.; Harutyunyan, B.; Neukirch, A. J.; Verduzco, R.; Crochet, J. J.; Tretiak, S.; Pedesseau, L.; Even, J.; Alam, M. A.; Gupta, G.; Lou, J.; Ajayan, P. M.; Bedzyk, M. J.; Kanatzidis, M. G.; Mohite, A. D. High-efficiency two-dimensional Ruddlesden−Popper perovskite solar cells. *Nature* **2016**, *536*, 312.

(2) Xing, G.; Mathews, N.; Lim, S. S.; Yantara, N.; Liu, X.; Sabba, D.; Grätzel, M.; Mhaisalkar, S.; Sum, T. C. Low-temperature solution-processed wavelength-tunable perovskites for lasing. *Nat. Mater.* **2014**, *13*, 476.

(3) Huang, H.; Bodnarchuk, M. I.; Kershaw, S. V.; Kovalenko, M. V.; Rogach, A. L. Lead Halide Perovskite Nanocrystals in the Research Spotlight: Stability and Defect Tolerance. *ACS Energy Lett.* **2017**, *2*, 2071−2083.

(4) Ke, W.; Kanatzidis, M. G. Prospects for low-toxicity lead-free perovskite solar cells. *Nat. Commun.* **2019**, *10*, 965.

(5) Akkerman, Q. A.; Rainò, G.; Kovalenko, M. V.; Manna, L. Genesis, challenges and opportunities for colloidal lead halide perovskite nanocrystals. *Nat. Mater.* **2018**, *17*, 394−405.

(6) Zhou, H.; Chen, Q.; Li, G.; Luo, S.; Song, T.-b.; Duan, H.-S.; Hong, Z.; You, J.; Liu, Y.; Yang, Y. Interface engineering of highly efficient perovskite solar cells. *Science* **2014**, *345* (6196), 542−546.

(7) Grätzel, M. The light and shade of perovskite solar cells. *Nat. Mater.* **2014**, *13*, 838.

(8) Tian, Y.; Zhou, C.; Worku, M.; Wang, X.; Ling, Y.; Gao, H.; Zhou, Y.; Miao, Y.; Guan, J.; Ma, B. Highly Efficient Spectrally Stable Red Perovskite Light-Emitting Diodes. *Adv. Mater.* **2018**, *30*, 1707093.

(9) Pan, J.; Quan, L. N.; Zhao, Y.; Peng, W.; Murali, B.; Sarmah, S. P.; Yuan, M.; Sinatra, L.; Alyami, N. M.; Liu, J.; Yassitepe, E.; Yang, Z.; Voznyy, O.; Comin, R.; Hedhili, M. N.; Mohammed, O. F.; Lu, Z. H.; Kim, D. H.; Sargent, E. H.; Bakr, O. M. Highly Efficient Perovskite-Quantum-Dot Light-Emitting Diodes by Surface Engineering. *Adv. Mater.* **2016**, *28*, 8718−8725.

(10) Liu, Y.; Cui, J.; Du, K.; Tian, H.; He, Z.; Zhou, Q.; Yang, Z.; Deng, Y.; Chen, D.; Zuo, X.; Ren, Y.; Wang, L.; Zhu, H.; Zhao, B.; Di, D.; Wang, J.; Friend, R. H.; Jin, Y. Efficient blue light-emitting diodes based on quantum-confined bromide perovskite nanostructures. *Nat. Photonics* **2019**, *13*, 760−764.

(11) Protesescu, L.; Yakunin, S.; Bodnarchuk, M. I.; Krieg, F.; Caputo, R.; Hendon, C. H.; Yang, R. X.; Walsh, A.; Kovalenko, M. V. Nanocrystals of Cesium Lead Halide Perovskites (CsPbX3, X = Cl, Br, and I): Novel Optoelectronic Materials Showing Bright Emission with Wide Color Gamut. *Nano Lett.* **2015**, *15*, 3692−3696.

(12) Talapin, D. V.; Lee, J. S.; Kovalenko, M. V.; Shevchenko, E. V. Prospects of Colloidal Nanocrystals for Electronic and Optoelectronic Applications. *Chem. Rev.* **2010**, *110*, 389−458.

(13) Boles, M. A.; Ling, D.; Hyeon, T.; Talapin, D. V. The surface science of nanocrystals. *Nat. Mater.* **2016**, *15*, 141−153.

(14) Kovalenko, M. V.; Protesescu, L.; Bodnarchuk, M. I. Properties and potential optoelectronic applications of lead halide perovskite nanocrystals. *Science* **2017**, *358* (6364), 745−750.

(15) Liu, Y.; Guo, M.; Dong, S.; Jiao, X.; Wang, T.; Chen, D. Room temperature colloidal synthesis of CsPbBr3 nanowires with tunable length, width and composition. *J. Mater. Chem. C* **2018**, *6*, 7797−7802.

(16) Kang, J.; Wang, L.-W. High Defect Tolerance in Lead Halide Perovskite CsPbBr3. *J. Phys. Chem. Lett.* **2017**, *8*, 489−493.

(17) Kobosko, S. M.; DuBose, J. T.; Kamat, P. V. Perovskite Photocatalysis. Methyl Viologen Induces Unusually Long-Lived Charge Carrier Separation in CsPbBr3 Nanocrystals. *ACS Energy Lett.* **2020**, *5*, 221−223.

(18) Hofmann, F. J.; Bodnarchuk, M. I.; Dirin, D. N.; Vogelsang, J.; Kovalenko, M. V.; Lupton, J. M. Energy Transfer from Perovskite Nanocrystals to Dye Molecules Does Not Occur by FRET. *Nano Lett.* **2019**, *19*, 8896−8902.

(19) Hofmann, F. J.; Bodnarchuk, M. I.; Protesescu, L.; Kovalenko, M. V.; Lupton, J. M.; Vogelsang, J. Exciton Gating and Triplet Deshelving in Single Dye Molecules Excited by Perovskite Nanocrystal FRET Antennae. *J. Phys. Chem. Lett.* **2019**, *10*, 1055−1062.

(20) Rossi, A.; Price, M. B.; Hardy, J.; Gorman, J.; Schmidt, T. W.; Davis, N. J. L. K. Energy Transfer between Perylene Diimide Based Ligands and Cesium Lead Bromide Perovskite Nanocrystals. *J. Phys. Chem. C* **2020**, *124*, 3306−3313.

(21) Loiudice, A.; Saris, S.; Oveisi, E.; Alexander, D. T. L.; Buonsanti, R. CsPbBr3 QD/AlOx Inorganic Nanocomposites with Exceptional Stability in Water, Light, and Heat. *Angew. Chem., Int. Ed.* **2017**, *56*, 10696−10701.

(22) Raja, S. N.; Bekenstein, Y.; Koc, M. A.; Fischer, S.; Zhang, D.; Lin, L.; Ritchie, R. O.; Yang, P.; Alivisatos, A. P. Encapsulation of Perovskite Nanocrystals into Macroscale Polymer Matrices: Enhanced Stability and Polarization. *ACS Appl. Mater. Interfaces* **2016**, *8*, 35523−35533.

(23) Liu, Y.; Li, F.; Liu, Q.; Xia, Z. Synergetic Effect of Postsynthetic Water Treatment on the Enhanced Photoluminescence and Stability of CsPbX3 (X = Cl, Br, I) Perovskite Nanocrystals. *Chem. Mater.* **2018**, *30*, 6922−6929.

(24) De Roo, J.; Ibáñez, M.; Geiregat, P.; Nedelcu, G.; Walravens, W.; Maes, J.; Martins, J. C.; Van Driessche, I.; Kovalenko, M. V.; Hens, Z. Highly Dynamic Ligand Binding and Light Absorption Coefficient of Cesium Lead Bromide Perovskite Nanocrystals. *ACS Nano* **2016**, *10*, 2071−2081.

(25) Pan, J.; Shang, Y.; Yin, J.; De Bastiani, M.; Peng, W.; Dursun, I.; Sinatra, L.; El-Zohry, A. M.; Hedhili, M. N.; Emwas, A.-H.; Mohammed, O. F.; Ning, Z.; Bakr, O. M. Bidentate Ligand-Passivated CsPbI3 Perovskite Nanocrystals for Stable Near-Unity Photoluminescence Quantum Yield and Efficient Red Light-Emitting Diodes. *J. Am. Chem. Soc.* **2018**, *140*, 562−565.

(26) Wei, Y.; Deng, X.; Xie, Z.; Cai, X.; Liang, S.; Ma, P. a.; Hou, Z.; Cheng, Z.; Lin, J. Enhancing the Stability of Perovskite Quantum Dots by Encapsulation in Crosslinked Polystyrene Beads via a Swelling−Shrinking Strategy toward Superior Water Resistance. *Adv. Funct. Mater.* **2017**, *27*, 1703535.

(27) Krieg, F.; Ochsenbein, S. T.; Yakunin, S.; ten Brinck, S.; Aellen, P.; Süess, A.; Clerc, B.; Guggisberg, D.; Nazarenko, O.; Shynkarenko, Y.; Kumar, S.; Shih, C.-J.; Infante, I.; Kovalenko, M. V. Colloidal CsPbX3 (X = Cl, Br, I) Nanocrystals 2.0: Zwitterionic Capping Ligands for Improved Durability and Stability. *ACS Energy Lett.* **2018**, *3*, 641−646.

(28) Krieg, F.; Ong, Q. K.; Burian, M.; Rainò, G.; Naumenko, D.; Amenitsch, H.; Süess, A.; Grotevent, M. J.; Krumeich, F.; Bodnarchuk, M. I.; Shorubalko, I.; Stellacci, F.; Kovalenko, M. V. Stable Ultraconcentrated and Ultradilute Colloids of CsPbX3 (X = Cl, Br) Nanocrystals Using Natural Lecithin as a Capping Ligand. *J. Am. Chem. Soc.* **2019**, *141*, 19839−19849.

(29) Tan, Y.; Zou, Y.; Wu, L.; Huang, Q.; Yang, D.; Chen, M.; Ban, M.; Wu, C.; Wu, T.; Bai, S.; Song, T.; Zhang, Q.; Sun, B. Highly Luminescent and Stable Perovskite Nanocrystals with Octylphosphonic Acid as a Ligand for Efficient Light-Emitting Diodes. *ACS Appl. Mater. Interfaces* **2018**, *10*, 3784−3792.

(30) Huang, H.; Chen, B.; Wang, Z.; Hung, T. F.; Susha, A. S.; Zhong, H.; Rogach, A. L. Water resistant CsPbX3 nanocrystals coated with polyhedral oligomeric silsesquioxane and their use as solid state

https://dx.doi.org/10.1021/jacs.0c03682
J. Am. Chem. Soc. 2020, 142, 12669−12680

luminophores in all-perovskite white light-emitting devices. *Chem. Sci.* **2016**, *7*, 5699−5703.
(31) Wang, W.; Aldeek, F.; Ji, X.; Zeng, B. R.; Mattoussi, H. A multifunctional amphiphilic polymer as a platform for surface-functionalizing metallic and other inorganic nanostructures. *Faraday Discuss.* **2014**, *175*, 137−151.
(32) Wang, W.; Kapur, A.; Ji, X.; Safi, M.; Palui, G.; Palomo, V.; Dawson, P. E.; Mattoussi, H. Photoligation of an Amphiphilic Polymer with Mixed Coordination Provides Compact and Reactive Quantum Dots. *J. Am. Chem. Soc.* **2015**, *137*, 5438−5451.
(33) Wang, W.; Ji, X.; Kapur, A.; Zhang, C.; Mattoussi, H. A Multifunctional Polymer Combining the Imidazole and Zwitterion Motifs as a Biocompatible Compact Coating for Quantum Dots. *J. Am. Chem. Soc.* **2015**, *137*, 14158−14172.
(34) Wang, W.; Ji, X.; Du, L.; Mattoussi, H. Enhanced Colloidal Stability of Various Gold Nanostructures Using a Multicoordinating Polymer Coating. *J. Phys. Chem. C* **2017**, *121*, 22901−22913.
(35) Jin, Z.; Du, L.; Zhang, C.; Sugiyama, Y.; Wang, W.; Palui, G.; Wang, S.; Mattoussi, H. Modification of Poly(maleic anhydride)-Based Polymers with H2N−R Nucleophiles: Addition or Substitution Reaction? *Bioconjugate Chem.* **2019**, *30*, 871−880.
(36) Jin, Z.; Kapur, A.; Wang, W.; Diaz Hernandez, J.; Thakur, M.; Mattoussi, H. The dual−function of lipoic acid groups as surface anchors and sulfhydryl reactive sites on polymer−stabilized QDs and Au nanocolloids. *J. Chem. Phys.* **2019**, *151*, 164703.
(37) De Roo, J.; Coucke, S.; Rijckaert, H.; De Keukeleere, K.; Sinnaeve, D.; Hens, Z.; Martins, J. C.; Van Driessche, I. Amino Acid-Based Stabilization of Oxide Nanocrystals in Polar Media: From Insight in Ligand Exchange to Solution 1H NMR Probing of Short-Chained Adsorbates. *Langmuir* **2016**, *32*, 1962−1970.
(38) Maes, J.; Balcaen, L.; Drijvers, E.; Zhao, Q.; De Roo, J.; Vantomme, A.; Vanhaecke, F.; Geiregat, P.; Hens, Z. Light Absorption Coefficient of CsPbBr3 Perovskite Nanocrystals. *J. Phys. Chem. Lett.* **2018**, *9*, 3093−3097.
(39) Mattoussi, H.; Mauro, J. M.; Goldman, E. R.; Anderson, G. P.; Sundar, V. C.; Mikulec, F. V.; Bawendi, M. G. Self-assembly of CdSe-ZnS quantum dot bioconjugates using an engineered recombinant protein. *J. Am. Chem. Soc.* **2000**, *122*, 12142−12150.
(40) Zhan, N.; Palui, G.; Mattoussi, H. Preparation of compact biocompatible quantum dots using multicoordinating molecular-scale ligands based on a zwitterionic hydrophilic motif and lipoic acid anchors. *Nat. Protoc.* **2015**, *10*, 859−874.
(41) Palui, G.; Avellini, T.; Zhan, N.; Pan, F.; Gray, D.; Alabugin, I.; Mattoussi, H. Photoinduced Phase Transfer of Luminescent Quantum Dots to Polar and Aqueous Media. *J. Am. Chem. Soc.* **2012**, *134*, 16370−16378.
(42) Susumu, K.; Uyeda, H. T.; Medintz, I. L.; Pons, T.; Delehanty, J. B.; Mattoussi, H. Enhancing the stability and biological functionalities of quantum dots via compact multifunctional ligands. *J. Am. Chem. Soc.* **2007**, *129*, 13987−13996.
(43) Imran, M.; Ijaz, P.; Goldoni, L.; Maggioni, D.; Petralanda, U.; Prato, M.; Almeida, G.; Infante, I.; Manna, L. Simultaneous Cationic and Anionic Ligand Exchange For Colloidally Stable CsPbBr3 Nanocrystals. *ACS Energy Lett.* **2019**, *4*, 819−824.
(44) Koscher, B. A.; Swabeck, J. K.; Bronstein, N. D.; Alivisatos, A. P. Essentially Trap-Free CsPbBr3 Colloidal Nanocrystals by Postsynthetic Thiocyanate Surface Treatment. *J. Am. Chem. Soc.* **2017**, *139*, 6566−6569.
(45) MØLler, C. K. Crystal Structure and Photoconductivity of Cæsium Plumbohalides. *Nature* **1958**, *182* (4647), 1436−1436.
(46) Bekenstein, Y.; Koscher, B. A.; Eaton, S. W.; Yang, P.; Alivisatos, A. P. Highly Luminescent Colloidal Nanoplates of Perovskite Cesium Lead Halide and Their Oriented Assemblies. *J. Am. Chem. Soc.* **2015**, *137*, 16008−16011.
(47) Swarnkar, A.; Chulliyil, R.; Ravi, V. K.; Irfanullah, M.; Chowdhury, A.; Nag, A. Colloidal CsPbBr3 Perovskite Nanocrystals: Luminescence beyond Traditional Quantum Dots. *Angew. Chem., Int. Ed.* **2015**, *54*, 15424−15428.
(48) Brennan, M. C.; Kuno, M.; Rouvimov, S. Crystal Structure of Individual CsPbBr3 Perovskite Nanocubes. *Inorg. Chem.* **2019**, *58*, 1555−1560.
(49) Cottingham, P.; Brutchey, R. L. On the crystal structure of colloidally prepared CsPbBr3 quantum dots. *Chem. Commun.* **2016**, *52*, 5246−5249.
(50) Cottingham, P.; Brutchey, R. L. Depressed Phase Transitions and Thermally Persistent Local Distortions in CsPbBr3 Quantum Dots. *Chem. Mater.* **2018**, *30*, 6711−6716.
(51) Bertolotti, F.; Protesescu, L.; Kovalenko, M. V.; Yakunin, S.; Cervellino, A.; Billinge, S. J. L.; Terban, M. W.; Pedersen, J. S.; Masciocchi, N.; Guagliardi, A. Coherent Nanotwins and Dynamic Disorder in Cesium Lead Halide Perovskite Nanocrystals. *ACS Nano* **2017**, *11*, 3819−3831.
(52) Zhao, Y.; Wei, J.; Li, H.; Yan, Y.; Zhou, W.; Yu, D.; Zhao, Q. A polymer scaffold for self-healing perovskite solar cells. *Nat. Commun.* **2016**, *7*, 10228.
(53) Kim, M.; Motti, S. G.; Sorrentino, R.; Petrozza, A. Enhanced solar cell stability by hygroscopic polymer passivation of metal halide perovskite thin film. *Energy Environ. Sci.* **2018**, *11*, 2609−2619.
(54) Colthup, N. B.; Daly, L. H.; Wiberley, S. E. In *Introduction to Infrared and Raman Spectroscopy*, 3rd ed.; Colthup, N. B., Daly, L. H., Wiberley, S. E., Eds.; Academic Press: San Diego, CA, 1990.
(55) Demillo, V. G.; Zhu, X. Zwitterionic amphiphile coated magnetofluorescent nanoparticles − synthesis, characterization and tumor cell targeting. *J. Mater. Chem. B* **2015**, *3*, 8328−8336.
(56) Choi, J.; Park, S.; Stojanović, Z.; Han, H.-S.; Lee, J.; Seok, H. K.; Uskoković, D.; Lee, K. H. Facile Solvothermal Preparation of Monodisperse Gold Nanoparticles and Their Engineered Assembly of Ferritin−Gold Nanoclusters. *Langmuir* **2013**, *29*, 15698−15703.
(57) Berne, B. J.; Pecora, R. *Dynamic Light Scattering: With Applications to Chemistry, Biology, and Physics*; Dover Publications: Mineola, NY, 2000; p vii.
(58) Nenon, D. P.; Pressler, K.; Kang, J.; Koscher, B. A.; Olshansky, J. H.; Osowiecki, W. T.; Koc, M. A.; Wang, L.-W.; Alivisatos, A. P. Design Principles for Trap-Free CsPbX3 Nanocrystals: Enumerating and Eliminating Surface Halide Vacancies with Softer Lewis Bases. *J. Am. Chem. Soc.* **2018**, *140*, 17760−17772.
(59) Kim, H.; Hight-Huf, N.; Kang, J.-H.; Bisnoff, P.; Sundararajan, S.; Thompson, T.; Barnes, M.; Hayward, R.; Emrick, T. S. Polymer Zwitterions for Stabilization of CsPbBr3 Perovskite Nanoparticle and Nanocomposite Films. *Angew. Chem., Int. Ed.* **2020**, *59*, 10802−10806.
(60) Meyns, M.; Perálvarez, M.; Heuer-Jungemann, A.; Hertog, W.; Ibáñez, M.; Nafria, R.; Genç, A.; Arbiol, J.; Kovalenko, M. V.; Carreras, J.; Cabot, A.; Kanaras, A. G. Polymer-Enhanced Stability of Inorganic Perovskite Nanocrystals and Their Application in Color Conversion LEDs. *ACS Appl. Mater. Interfaces* **2016**, *8*, 19579−19586.
(61) Baranov, D.; Caputo, G.; Goldoni, L.; Dang, Z.; Scarfiello, R.; De Trizio, L.; Portone, A.; Fabbri, F.; Camposeo, A.; Pisignano, D.; Manna, L. Transforming colloidal Cs4PbBr6 nanocrystals with poly(maleic anhydride-alt-1-octadecene) into stable CsPbBr3 perovskite emitters through intermediate heterostructures. *Chem. Sci.* **2020**, *11*, 3986−3995.
(62) Bodnarchuk, M. I.; Boehme, S. C.; ten Brinck, S.; Bernasconi, C.; Shynkarenko, Y.; Krieg, F.; Widmer, R.; Aeschlimann, B.; Günther, D.; Kovalenko, M. V.; Infante, I. Rationalizing and Controlling the Surface Structure and Electronic Passivation of Cesium Lead Halide Nanocrystals. *ACS Energy Lett.* **2019**, *4*, 63−74.
(63) Chen, Y.; Smock, S. R.; Flintgruber, A. H.; Perras, F. A.; Brutchey, R. L.; Rossini, A. J. Surface Termination of CsPbBr3 Perovskite Quantum Dots Determined by Solid-State NMR Spectroscopy. *J. Am. Chem. Soc.* **2020**, *142*, 6117−6127.
(64) Kim, G.; Yoo, C. E.; Kim, M.; Kang, H. J.; Park, D.; Lee, M.; Huh, N. Noble Polymeric Surface Conjugated with Zwitterionic Moieties and Antibodies for the Isolation of Exosomes from Human Serum. *Bioconjugate Chem.* **2012**, *23*, 2114−2120.

(65) Susumu, K.; Mei, B. C.; Mattoussi, H. Multifunctional ligands based on dihydrolipoic acid and polyethylene glycol to promote biocompatibility of quantum dots. *Nat. Protoc.* **2009**, *4*, 424−436.
(66) Mei, B. C.; Susumu, K.; Medintz, I. L.; Mattoussi, H. Polyethylene glycol-based bidentate ligands to enhance quantum dot and gold nanoparticle stability in biological media. *Nat. Protoc.* **2009**, *4*, 412−423.
(67) Mei, B. C.; Susumu, K.; Medintz, I. L.; Delehanty, J. B.; Mountziaris, T. J.; Mattoussi, H. Modular poly(ethylene glycol) ligands for biocompatible semiconductor and gold nanocrystals with extended pH and ionic stability. *J. Mater. Chem.* **2008**, *18*, 4949−4958.

https://dx.doi.org/10.1021/jacs.0c03682
J. Am. Chem. Soc. 2020, 142, 12669−12680